

Ultrafast Photodissociation Dynamics of Nitromethane

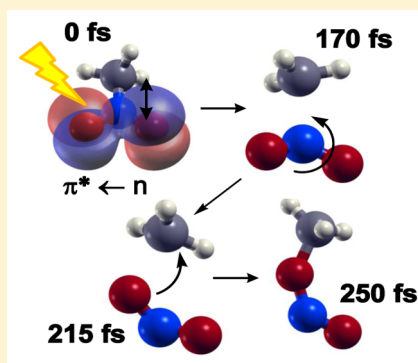
Tammie Nelson,^{†,‡} Josiah Bjorgaard,^{†,‡} Margo Greenfield,^{†,¶} Cindy Bolme,^{†,¶} Katie Brown,^{†,¶} Shawn McGrane,^{†,¶} R. Jason Scharff,^{*,†,¶} and Sergei Tretiak^{*,†,‡}

[†]Los Alamos National Laboratory, Los Alamos, New Mexico 87545, United States

[‡]Theoretical Division, Physics and Chemistry of Materials (T-1) and [¶]Explosive Science and Shock Physics Division, Shock and Detonation Physics (M-9), Los Alamos National Laboratory, Los Alamos, New Mexico 87545, United States

Supporting Information

ABSTRACT: Nitromethane (NM), a high explosive (HE) with low sensitivity, is known to undergo photolysis upon ultraviolet (UV) irradiation. The optical transparency, homogeneity, and extensive study of NM make it an ideal system for studying photodissociation mechanisms in conventional HE materials. The photochemical processes involved in the decomposition of NM could be applied to the future design of controllable photoactive HE materials. In this study, the photodecomposition of NM from the $n\pi^*$ state excited at 266 nm is being investigated on the femtosecond time scale. UV femtosecond transient absorption (TA) spectroscopy and excited state femtosecond stimulated Raman spectroscopy (FSRS) are combined with nonadiabatic excited state molecular dynamics (NA-ESMD) simulations to provide a unified picture of NM photodecomposition. The FSRS spectrum of the photoproduct exhibits peaks in the NO_2 region and slightly shifted C–N vibrational peaks pointing to methyl nitrite formation as the dominant photoproduct. A total photolysis quantum yield of 0.27 and an $n\pi^*$ state lifetime of ~ 20 fs were predicted from NA-ESMD simulations. Predicted time scales revealed that NO_2 dissociation occurs in 81 ± 4 fs and methyl nitrite formation is much slower having a time scale of 452 ± 9 fs corresponding to the excited state absorption feature with a decay of 480 ± 17 fs observed in the TA spectrum. Although simulations predict C–N bond cleavage as the primary photochemical process, the relative time scales are consistent with isomerization occurring via NO_2 dissociation and subsequent rebinding of the methyl radical and nitrogen dioxide.



INTRODUCTION

As a low-sensitivity high explosive (HE), nitromethane (NM [H_3CNO_2]) has become widely recognized as an ideal system for studying the chemical mechanisms associated with conventional explosive initiation and subsequent detonation. Numerous studies to investigate the fundamental processes involved in initiation and detonation have been performed on NM including shock-induced vibrational heating and energy transfer,^{1,2} thermal and impact induced decomposition,^{3,4} and shock wave dynamics.⁵ There is some evidence that the formation of NO_2 through homolytic bond cleavage is the critical first step that catalyzes the exothermic decomposition in the chain reaction leading to detonation.⁶ Other studies indicate more complex bimolecular reactions under pressure.^{7–9} The chemistry of initiation is complex and it has been conjectured that electronic excitations and photochemical pathways^{10,11} could be involved, going beyond the simple picture of thermal decomposition.¹²

In its current implementation, optical initiation of conventional explosives relies on indirect thermal or shock mechanisms^{13–15} that require high-powered lasers and offer little possibility of control over the reactive process. Direct optical initiation (also referred to as *photoinitiation*) is thought to be achievable through an excited state photodecomposition

mechanism in a properly designed photoactive HE whose excited state photochemical processes would lead to initiation. At this point, no conventional materials are known to undergo direct optical initiation. In addition to pyrolysis, NM also undergoes ultraviolet (UV) photolysis making it an ideal candidate for studying photodecomposition in HEs. Photodecomposition is a critical component in photoinitiation, therefore understanding this process may have implications for the design of novel photoactive HE materials used for direct optical initiation.¹⁶

Despite being the simplest nitroalkane, NM is endowed with surprisingly complex photochemistry and electronic structure. While its photodecomposition has been the subject of numerous experimental and theoretical investigations,^{17–30} a collective picture of dissociation dynamics remains elusive partly due to differing experimental conditions. The subpicosecond dynamics is of particular interest, as this is when photoproducts are initially formed. However, very few time-resolved experiments access the ultrafast time regime^{23,24} where

Received: October 6, 2015

Revised: December 11, 2015

Published: January 6, 2016

the photoproduct intermediates may differ considerably from species observed at picosecond or nanosecond time scales.

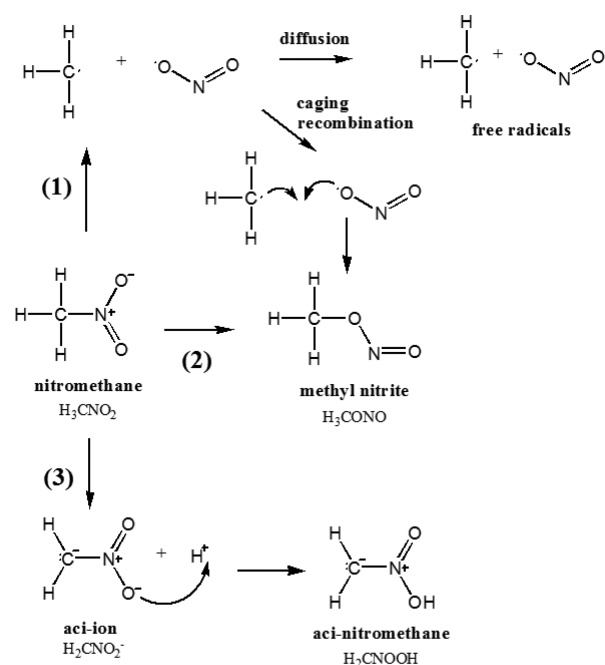
From the theoretical perspective, the ground and excited electronic potential energy surfaces (PES) involved in NM decomposition have been rigorously characterized.^{26–29} PES mapping is an important tool that allows photochemical pathways and photoproducts to be predicted as well as provides mechanistic insights that probe the role of conical intersections²⁸ and identify transition states.^{29,30} However, the static description does not provide chemical reaction branching ratios, quantum yields, time scales, or excited state lifetimes. For that purpose, molecular dynamics (MD) incorporating quantum transitions must be performed. Classical force field MD has commonly been used to study shock induced and thermally induced decomposition in the ground electronic state. On the other hand, the use of excited state MD, essential to understanding the role of electronic excitations and photochemistry, has not enjoyed the same popularity.

The formation of NO₂ through C–N bond rupture described by



as shown in reaction (1) of Scheme 1 is generally agreed to be the primary photolysis process^{24,31,32} after excitation of either

Scheme 1. Scheme Depicting Nitromethane, Possible Reaction Pathways, and Photoproducts



the $\pi^* \leftarrow \pi$ or $\pi^* \leftarrow n$ transitions in NM. Among the various secondary reaction pathways, infrared (IR) multiphoton dissociation experiments of NM have shown that nitro-nitrite isomerization given by



as shown in reaction (2) of Scheme 1 is competitive with the rupture of the C–N bond.²⁰ Pimentel et al.¹⁷ have shown that nitro-nitrite isomerization is the primary process in the formation of the HNO radical which has been observed in the photolysis of NM in solid argon at 20 K. It is suggested that methyl nitrite formation results from the recombination of the

methyl radical and nitrogen dioxide¹⁸ (see Scheme 1) although the exact nature of the transition state is still under debate.^{29,30} The well-known aci-ion (H₂CNO₂⁻) and related aci-nitromethane (H₂CNOOH) are shown in reaction (3) of Scheme 1 and will be discussed later in more detail.

In this work, we perform simultaneous UV femtosecond (fs) transient absorption (TA) spectroscopy and excited state femtosecond stimulated Raman spectroscopy (FSRS) to characterize the dynamical ultrafast optical response of the $n\pi^*$ state of NM excited at 266 nm. Our experiments provide new mechanistic insights into the $n\pi^*$ photodissociation pathway of NM on the fs time scale and support the “roaming pathway” hypothesis³⁰ of methyl nitrite formation. Experimental findings are verified using nonadiabatic excited state molecular dynamics (NA-ESMD)^{33,34} to model the non-radiative relaxation through the manifold of excited states in NM following excitation to the $n\pi^*$ state. Dynamics on the actual excited state PESs allows the internal conversion to be followed as excess electronic energy is converted into vibrational energy resulting in nuclear motions and bond cleavage. We verify that NA-ESMD (a trajectory surface hopping method) can be used effectively to model photochemistry, and also provides $n\pi^*$ state lifetime, quantum yield, and, for the first time, relative time scales for photochemical pathways in NM.

EXPERIMENTAL METHODS

A 266 nm 50 fs laser pulse was used to access the $\pi^* \leftarrow n$ transition of neat NM. The dynamic optical response of NM was characterized by simultaneous transient absorption (TA) spectroscopy across the 410–480 nm spectral range and excited state femtosecond stimulated Raman spectroscopy (FSRS). The laser employed in this work was a Ti:sapphire Coherent Micra oscillator and Legend USX-HE amplifier. A 33% beamsplitter was used to separate the 1 kHz 2.0 mJ 800 nm pulse into pump and probe beams. The higher energy, pump was frequency doubled and then 400 and 800 nm were mixed in a BBO crystal to create 266 nm light. The 266 nm pump beam was sent through an acousto-optical modulator pulse shaper that consisted of a 4-f zero dispersion compressor.³⁵ The lower energy probe beam was split with a 90% beam splitter to make a white light supercontinuum (375–750 nm) and narrow band 406 nm beam. The supercontinuum was produced by focusing a spatially selected (through an iris), bandwidth selected (20 nm bandpass, 810 nm central wavelength filter), and attenuated fraction of the 10% 800 nm probe pulse into a 2 mm quartz cuvette of deionized water. The remaining 90% 800 nm light was passed through a 6 mm thick type-one BBO crystal and two narrow band filters to create a 406 nm pulse with a Full Width at Half-Maximum (FWHM) of ~0.7 nm.

Transient Absorption (TA). TA requires two femtosecond laser pulses: the 2 μJ 266 nm pump pulse and the nJ supercontinuum probe pulse (375–750 nm). The 266 nm pump pulse promotes a fraction of the molecules to an electronically excited state to initiate photochemical dynamics. The time delay between the pump and probe pulse is scanned, and for each time delay, the intensities of the probe pulse are recorded with and without the pump pulse. A differential absorption [$\Delta A(\lambda, t)$] spectrum was computed from the absorption spectrum of the excited sample (with pump pulse) minus the ground state absorption of the sample (without pump pulse). The frequency-dependent delay, or chirp, of the supercontinuum was corrected numerically, which

causes small artifacts due to the 50 fs delay steps. The white light continuum chirp was removed by numerically finding the maximum apparent transient absorption signal which appears when pulses overlap in time and shifting the time axis to place this at $t = 0$. Due to the 50 fs time step and the 250 fs chirp over the spectral range, there are 5 such shifts in time causing the apparent jumps in the spectral axis. The lifetime was determined using a narrow spectral range where no shifting occurred by fitting the TA signal to an exponential decay with an offset. The lifetime did not depend on the wavelength in this spectral range, indicating that the temporal step size of 50 fs is sufficient.

Difference Femtosecond Stimulated Raman Spectroscopy (d-FSRS). FSRS uses two pulses: a narrow bandwidth (<1 ps, 35–45 cm^{-1} , 5–10 μJ , 406 nm) Raman pump pulse and a supercontinuum Stokes probe pulse (0.25 ps chirped, 408–480 nm, < 20 nJ). The probe pulse is red-shifted with respect to the pump providing a Stokes field overlapping the 200–4000 cm^{-1} vibrational range. Raman gain features on top of the continuum probe spectrum can be observed when the pump and probe pulses interact simultaneously with the sample causing stimulated Raman transitions that are related to the bond specific vibrational modes of the sample. To probe the time-resolved vibrational structure of the electronically excited sample, the delay between the 266 nm pump (actinic pump) and the FSRS probe was scanned. The difference between the FSRS signal with and without the pump pulse is denoted as the difference FSRS (d-FSRS). The FSRS, d-FSRS, TA, and supercontinuum spectra were each recorded at 250 Hz by using 2 optical choppers.

Together with the TA spectrum, the Raman spectrum provides a description of the excited state dynamics, and enables us to directly probe NM photochemistry (NO_2 formation, aci-ion [H_2CNO_2^-] formation, oxygen dissociation, or methyl nitrite [H_3CONO] formation).

■ COMPUTATIONAL METHODS AND SIMULATION DETAILS

The previously developed nonadiabatic excited-state molecular dynamics (NA-ESMD) framework^{33,34,36–39} was used to investigate photoexcited dynamics of NM. NA-ESMD uses the fewest-switches surface hopping (FSSH)⁴⁰ algorithm to follow dynamics occurring on multiple coupled electronic excited states following photoexcitation. Briefly, FSSH is a mixed quantum classical approach in which nuclei are treated classically and are propagated according to forces from a single adiabatic excited state at any given time. Transitions from one excited state to another occur stochastically⁴¹ based on the nonadiabatic coupling strengths. Meanwhile, electrons have a quantum mechanical description related to excited state energies, gradients, and nonadiabatic coupling terms which are computed “on the fly” analytically.^{33,42–46} Electronic excited states are calculated with the collective electronic oscillator (CEO) approach^{47,48} using the configuration interaction singles (CIS) formalism⁴⁹ implemented with the semiempirical Austin Model 1 (AM1) Hamiltonian.⁵⁰

The AM1 electronic structure representation provides a good description of ground electronic state properties. This was verified for NM by computing the ground state (GS) bond dissociation energy for the C–N bond ($\text{CH}_3\text{–NO}_2 \rightarrow \text{CH}_3^+ + \text{NO}_2^-$) in solution giving 61.1 kcal/mol in good agreement with the gas phase measurement of 60.1 kcal/mol.³ Furthermore, we calculate an S_1 vertical transition energy of 348 nm for a single

molecule in solution. Previous single-molecule ab initio quantum chemistry calculations assign a CAS SCF gap of 326 nm.⁵¹

Our modeling approach allows the dynamics of a photoexcited wavepacket to be followed as the system relaxes nonradiatively from an initial high energy electronic excited state back to the lowest energy excited state S_1 . Simulations were performed according to the following. Starting from the AM1 optimized GS geometry, molecular dynamics in the ground electronic state was performed for 300 ps using a time step of $\Delta t = 0.5$ fs and constant-temperature Langevin dynamics⁵² to equilibrate to a temperature of 300 K using a friction coefficient of 2.0 ps^{-1} . From this trajectory, 580 snapshots were collected at 500 fs intervals to provide an ensemble of initial ground-state configurations and momenta.

For each initial configuration, oscillator strengths and vertical excitation energies for the 13 lowest energy excited states were computed using the CEO method in order to construct the equilibrated linear absorption spectrum. This was done by making a histogram of the excited state energies in which the height of the histogram is related to the average optical absorbance at a given wavelength⁵³ for the corresponding state. Dominating contributions to the molecular orbitals were calculated using the Gaussian 09 software package⁵⁴ at the CIS/AM1 level of theory for the vertical excitations from the AM1 optimized GS geometry. The $\pi^* \leftarrow n$ transition was chosen as the initial excitation according to a Franck–Condon window centered at 200 nm (see Results section) with a Gaussian temporal profile corresponding to a FWHM of 100 fs. The NA-ESMD simulations of isolated molecules were then started from the different photoexcited configurations where the $n\pi^*$ state corresponds to S_4 – S_7 due to conformational disorder. Each independent trajectory was propagated using energy conserving Newtonian dynamics for 2 ps with a classical time step of $\Delta t = 0.1$ fs and a quantum time step of $\delta t = 0.025$ fs. Trivial unavoided crossings were located³⁷ by further reducing the quantum time step by a factor of 10, and electronic decoherence was included using the instantaneous decoherence correction.³⁹ A total of 417 converged trajectories were obtained which were then used to statistically compute excited state lifetimes and quantum yields. Details of our analysis in assigning trajectories as dissociative or non-dissociative can be found in the Supporting Information.

■ RESULTS

Optical Spectra and Excited State Lifetime. The computed linear absorption spectrum for gas-phase NM is shown in Figure 1 where the individual contributions from each state are also shown. The experimental UV absorption spectrum shown in the inset of Figure 1 was recorded for a 0.01 M NM solution in water. While the computed spectrum shows a uniform blue shift of 50 nm with respect to the experimental spectrum, the spectral features and their relative energy difference are reproduced by the chosen level of theory. For NA-ESMD simulations, rather than the absolute energy, the energy difference is the relevant factor related to the strength of the nonadiabatic coupling and thus the relaxation rate. Nitromethane is known to exhibit the $\pi^* \leftarrow n$ transition in a weak-band at 270 nm⁵⁵ while a stronger absorption band at 198 nm is associated with the $\pi^* \leftarrow \pi$ transition.⁵⁶ Therefore, we can assign the peaks in the theoretical spectrum at 220 nm to the $n\pi^*$ state and 150 nm to the $\pi\pi^*$ state. Indeed, this can be verified by molecular orbital analysis shown schematically in

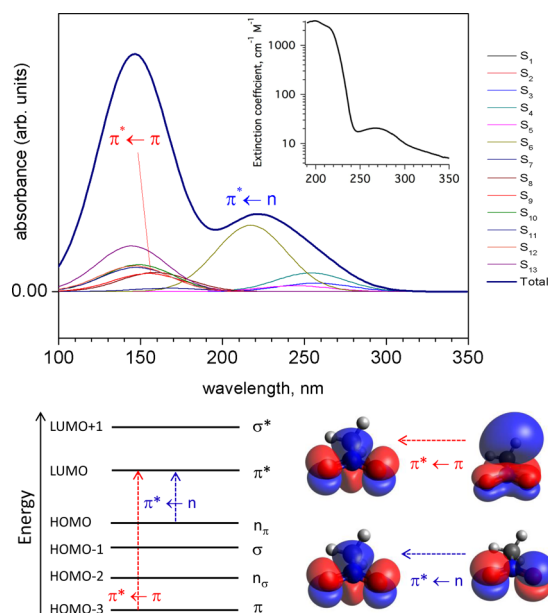


Figure 1. (Top) Computed gas-phase equilibrated absorption spectrum where contributions from the 13 lowest energy excited states have been included for nitromethane at 300 K. The $n\pi^*$ and $\pi\pi^*$ transitions are labeled at 220 and 150 nm, respectively. The experimental UV absorption spectrum recorded at 0.01 M solution in water is shown in the inset. (Bottom) Schematic energy diagram and molecular orbitals of relevant transitions.

Figure 1. As can be seen, the $n\pi^*$ state at 220 nm corresponds to a HOMO \rightarrow LUMO transition from the nonbonding oxygen electrons to a NO_2 π orbital, and the $\pi\pi^*$ state localized on NO_2 arises from a HOMO-3 \rightarrow LUMO transition. Lower energy transitions appearing near 255 nm in the computed spectrum correspond to $n\sigma^*$ transitions and have relatively small oscillator strength.

The evolution of the adiabatic state populations during NA-ESMD simulations can be followed in **Figure 2**. The populations are computed as the fraction of trajectories

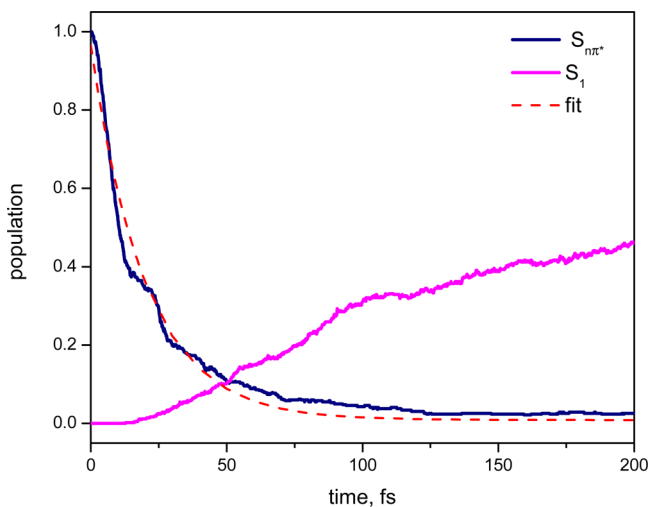


Figure 2. Time evolution of adiabatic state populations (fraction of trajectories) during NA-ESMD simulations showing the transfer of population from the initial $n\pi^*$ state (blue) to the lowest energy S_1 state (pink). The initial $n\pi^*$ state population is fit to exponential decay function (red dashes) to determine the lifetime of the $n\pi^*$ state.

evolving on a certain state at any given time. The initially excited $n\pi^*$ state population decays as the system relaxes to the lowest energy S_1 excited state where the population increases. The $n\pi^*$ state population can be fit to a simple exponential decay function (shown in **Figure 2** in red dashes) with the form $f(x) = A \exp(-x/\tau_{n\pi^*}) + y_0$ where $\tau_{n\pi^*}$ represents the $n\pi^*$ state lifetime. Rajchenbach²² reported an excited state lifetime of nitromethane pumped with 299 nm of ≤ 1 ps. A significantly shorter $n\pi^*$ state lifetime of 36 ± 5 fs for excitation at 271 nm was later measured by Guo.²⁴ We obtain a value of $\tau_{n\pi^*} = 20.10 \pm 0.04$ fs from the fit which supports the previously reported sub-100 fs $n\pi^*$ state lifetime. The TA signal, seen in the top panel of **Figure 3**, was fit to an exponential decay function of

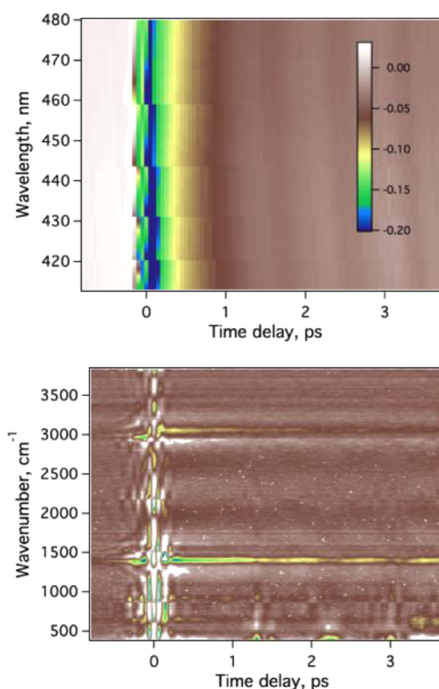


Figure 3. Transient absorption (top) and d-FSRS (bottom) in nitromethane excited by 50 fs 266 nm pulses.

the form $f(x) = A \exp(-x/\tau) + y_0$ with lifetime τ . In the neat liquid, the initial increase in transient absorption decayed with a lifetime of 480 ± 17 fs.

Photodissociation Pathways. The d-FSRS results shown in the bottom of **Figure 3** demonstrate that only minor changes are observed after the initial excitation. We cannot clearly resolve vibrational changes at times < 200 fs, and only minor spectral evolution occurs at times longer than 200 fs. We have measured TA and d-FSRS to times > 150 ps, as reported earlier.⁵⁷ **Figure 4** shows the FSRS and d-FSRS spectrum, along with the product spectrum obtained by adding 8.5% of the original NM FSRS spectrum to the d-FSRS to account for loss of reactants. The product spectrum exhibits a shifted peak in the C–N bond region signaling a C–O bond. There are still strong peaks in the NO_2 regions. The simplest interpretation of the d-FSRS photoproduct spectrum is an isomerization to methyl nitrite. This conversion appears to happen on a subpicosecond time scale, as no transient C–N bond breakage is apparent in the d-FSRS of **Figure 3** prior to formation of the final product.

We observe the main Raman peaks of the photoproduct at 885, 1310–1430 (broad), 1570, 1700, 2920, and 2980–3080

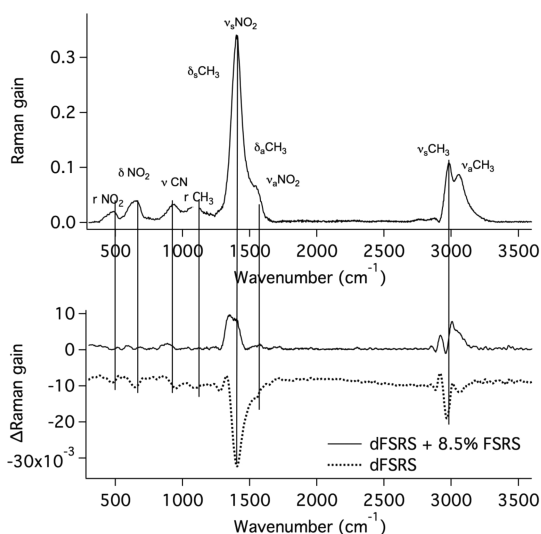


Figure 4. Femtosecond stimulated Raman of nitromethane (top) and long time change in signal (bottom, dashed line) and photoproduct spectrum (bottom, solid line).

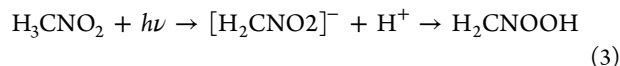
(broad). Smaller features are difficult to distinguish from noise, but may be present. There is no evidence of aci-ion (H_2CNO_2^-) Raman at 3335 cm^{-1} .⁵⁸ Furthermore, there are no peaks in the OH region ($3200\text{--}3700\text{ cm}^{-1}$) suggestive of HONO or CH_2NOOH . Dissociation into radicals would produce CH_3 ⁵⁹ with vibrational frequencies at ~ 617 (IR),⁶⁰ $1360\text{--}1420$ (IR, Raman),⁶⁰ 3002 (Raman),^{59,61} and 3108 broad (IR, Raman) cm^{-1} ,⁶² and NO_2 ⁶³ with ~ 750 (Raman), 1325 (Raman), and 1618 (IR) cm^{-1} . Dissociation into ions would produce CH_3^+ with peaks shifted to ~ 730 (IR),⁶⁴ 1385 (IR, Raman),⁶⁴ 3108 broad (IR, Raman),⁶⁵ and NO_2^- with peaks at ~ 827 (Raman) and 1325 (Raman) cm^{-1} .⁶³ The CH_3 peaks at ~ 1385 would shift to ~ 1020 with deuteration;⁶⁴ we observe the broad peak at 1400 cm^{-1} to remain unchanged upon full deuteration of the nitromethane, a clear signature that the peak is not due to CH_3 .

Methyl nitrite has strong IR absorptions at $\sim 550\text{--}650$, $780\text{--}875$, $950\text{--}1050$, and $1600\text{--}1700$, as well as weaker absorptions around $1340\text{--}1490$ and $2900\text{--}3070\text{ cm}^{-1}$.⁶⁶ There are peaks due to two isomers that interconvert at room temperature.⁶⁷ At ambient conditions, methyl nitrite is a gas that must be synthesized and purified with multiple cryogenic distillation steps.⁶⁸ We have not undertaken the production of methyl nitrite, and while there are no Raman results in the literature, we use the gas phase^{67,68} and matrix⁶⁶ IR methyl nitrite studies to compare to our data. If the Raman intensity of the peaks around 1400 (N=O stretch) and 3000 (C-H stretches) cm^{-1} are stronger than the IR activity, methyl nitrite is a reasonable assignment for our photoproduct. On the other hand, the photoproduct peak at 885 cm^{-1} is not well matched to methyl nitrite, and the weak peaks 1570 and 1700 cm^{-1} are also shifted from the expected 1650 cm^{-1} peak. We tentatively assign the photoproduct to methyl nitrite with a reasonable match to key spectral features measured in low temperature rare gas matrix, and due to the more decisive elimination of other likely photochemical pathways.

The primary photodissociation pathway observed during gas-phase NA-ESMD simulations was cleavage of the C–N bond according to reaction 1. The dissociation of NO_2 occurred in 101 trajectories giving a predicted quantum yield of 0.24. We also observed nitro-nitrite isomerization in NA-ESMD

simulations. This process is known to be a competitive pathway to C–N bond cleavage.²⁰ The production of methyl nitrite shown in reaction 2 was seen in 14 trajectories giving a predicted quantum yield of 0.03. For those trajectories that undergo methyl nitrite formation, the average maximum C–N bond distance was $3.0 \pm 0.2\text{ \AA}$. (See the Supporting Information for a description of the analysis used to assign pathways to the NA-ESMD trajectories.)

The final photodecomposition pathway that was observed in simulations was the formation of aci-nitromethane (H_2CNOOH), which is formed by migration of a hydrogen from the methyl center to one of the oxygen atoms of the nitro group according to



(See reaction (3) in Scheme 1). The aci-nitromethane species is involved in detonation sensitization and can be produced upon UV irradiation.²¹ Only 1 instance of this pathway was observed in our simulations corresponding to a relatively low quantum yield of 2.4×10^{-3} verifying that this is not the dominant $n\pi^*$ photoproduct.

We computed time scales for the two dominant photodissociation pathways observed in NA-ESMD simulations, specifically, C–N bond cleavage and methyl nitrite formation. To do this, we track the relevant bond lengths during dynamics considering only those trajectories that exhibit the pathway of interest. The evolution of the average separation distance can be seen in Figure 5 for the C–N bond (top panel of Figure 5),

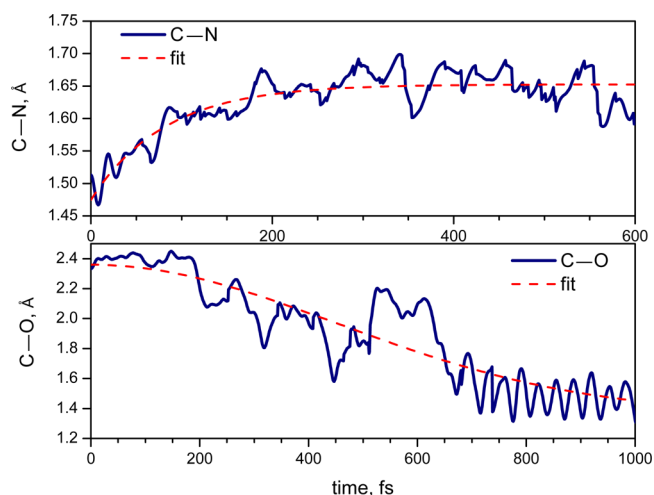


Figure 5. Average separation distance during NA-ESMD simulations for (top) C–N in trajectories that undergo NO_2 dissociation and (bottom) C–O in trajectories where the C–O bond forms during nitro-nitrite isomerization. Fits shown in red dashes are used to compute the time scales for the processes.

which breaks to produce NO_2 ($\text{H}_3\text{C-NO}_2$) in reaction 1 and the C–O bond (bottom panel of Figure 5) that forms during isomerization of the nitro group ($\text{H}_3\text{C-ONO}$) in reaction 2. As can be seen, the average C–N bond length increases as the bond stretches and breaks while the average C–O separation distance shortens as the new bond is formed (additional discussion of the average C–N separation distance can be found in Supporting Information). The time scale for NO_2 dissociation was computed by fitting the average C–N bond length evolution to a simple exponential growth function of the

Table 1. Theoretical Quantum Yields (QY), Time Scales, and Fitting Parameters for Predicted NM Photodissociation Pathways

pathway	QY	time scale, fs	y_0	A
NO ₂ dissociation	0.24	81 ± 4	1.653 ± 0.001	-0.178 ± 0.005
methyl nitrite formation	0.03	452 ± 9	1.37 ± 0.01	0.99 ± 0.01
aci-nitromethane formation	2.4 × 10 ⁻³			

form $f(x) = A \exp(x/\tau_{C-N}) + y_0$ where τ_{C-N} represents the lifetime of the C–N bond. Similarly, the average C–O bond length was fit to a Gaussian decay function of the form $f(x) = A \exp(-0.5(x/\tau_{C-O})^2) + y_0$ to determine the time scale for C–O bond formation represented by τ_{C-O} . We compute time scales of $\tau_{C-N} = 81 \pm 4$ fs for NO₂ dissociation and $\tau_{C-O} = 452 \pm 9$ fs for the nitro-nitrite isomerization. The fits are shown in Figure 5 in red dashes and the time scales and fitting parameters are provided in Table 1 along with the computed quantum yields for each pathway. Note that the time scale for aci-nitromethane (H₂CNOOH) formation could not be computed as there was not a large enough sample to compute a statistically relevant time scale. The predicted total photolysis quantum yield for $n\pi^*$ is 0.27 which agrees with the quantum yield at 299 nm of 0.24 ± 0.05 measured by Rajchenbach.²²

DISCUSSION

The apparent discrepancy between experimental observation of methyl nitrite as the primary photoproduct and the results of our NA-ESMD simulations, which predict the highest quantum yield for NO₂ dissociation, can be reconciled. NO₂ dissociation observed in gas phase NA-ESMD simulations can be interpreted as the first step of methyl nitrite formation. In solution, caging effects may promote rebinding of the dissociated NO₂ (see Scheme 1), similar to the caging mechanism observed for I₂ photodissociation in the solid matrix.^{69,70} The gas phase, by contrast, is less amenable to recombination as any dissociated NO₂ can quickly diffuse making the isomerization pathway difficult to observe in our simulations.

This mechanism is supported by the relative time scales for the two processes: NO₂ dissociation is predicted to occur on a very fast time scale of 81 ± 4 fs, whereas methyl nitrite formation is much slower having a time scale of 452 ± 9 fs. Note that this time scale is similar to the 480 ± 17 fs decay of TA reported here, with methyl nitrite as the apparent product observed in FSRS. NO₂ dissociation and subsequent rebinding in the nitrite arrangement is consistent with predicted time scales. Therefore, we expect that methyl nitrite formation in solution should be a dominant process. Furthermore, the 3.0 Å maximum C–N bond distance observed during isomerization supports the “roaming pathway” hypothesis.³⁰

CONCLUSION

To summarize, the ultrafast fs time scale photodissociation dynamics of the $n\pi^*$ transition at 266 nm in condensed liquid NM have been investigated by simultaneous UV transient absorption spectroscopy and excited state FSRS and d-FSRS. Gas-phase NA-ESMD simulations have also been used to model the photodissociation dynamics. The persistent strong peaks in the NO₂ regions and slight shifts between the FSRS and d-FSRS C–N vibrational peaks strongly suggest methyl nitrite as the primary photoproduct that is likely formed on a subpicosecond time scale. The TA spectrum shows an excited state absorption with a lifetime of 480 ± 17 fs consistent with the predicted time scale of 452 ± 9 fs for methyl nitrite

formation calculated from NA-ESMD simulations. NA-ESMD simulations predict an $n\pi^*$ total photolysis quantum yield of 0.27 and have confirmed the previously reported sub-100 fs $n\pi^*$ state lifetime. NO₂ dissociation was found to be relatively fast compared to the slower methyl nitrite formation consistent with isomerization through recombination of the methyl radical and nitrogen dioxide.

The present simulations provide confidence that NA-ESMD can be used successfully to model photochemistry and provide valuable mechanistic insights that often cannot be accessed by experiment alone. While the CIS electronic structure description used in the present NA-ESMD implementation provides a good description of crossings in the excited state manifold, it cannot follow crossings between the first excited state with the ground state. As a consequence, our reported results do not include hot ground state reactions that might affect the final photoproduct yields on longer time scales. Ongoing development of NA-ESMD methodology seeks to address this limitation as well as introduce spin state dynamics of photofragments in order to extend modeling in molecular photodissociation processes to longer time scales. Despite this limitation, we now have a combined experimental and theoretical toolbox that will allow us to determine relative time scales, quantum yields, photoproducts and intermediates, and mechanistic information that can be applied to the future design of novel photoactive HE materials and a variety of functional molecular systems undergoing photochemical reactions.

ASSOCIATED CONTENT

Supporting Information

The Supporting Information is available free of charge on the ACS Publications website at DOI: 10.1021/acs.jpca.5b09776.

We provide a description of the analysis used in order to assign NA-ESMD trajectories as dissociative or non-dissociative (PDF)

AUTHOR INFORMATION

Corresponding Authors

*E-mail: scharff@lanl.gov.

*E-mail: serg@lanl.gov.

Notes

The authors declare no competing financial interest.

ACKNOWLEDGMENTS

The authors acknowledge support from the Los Alamos National Laboratory (LANL) Directed Research and Development funds (LDRD). T.N. gratefully acknowledges support from the Richard P. Feynman Fellowship in Theory and Computing. This research used resources provided by the Los Alamos National Laboratory Institutional Computing Program. LANL is operated by Los Alamos National Security, LLC, for the National Nuclear Security Administration of the U.S. Department of Energy under contract DE-AC52-06NA25396. We acknowledge support of Center for Nonlinear Studies

(CNLS) and Center for Integrated Nanotechnology (CINT), a U.S. Department of Energy and Office of Basic Energy Sciences user facility.

REFERENCES

- (1) Dawes, R.; Siavosh-Haghighi, A.; Sewell, T. D.; Thompson, D. L. Shock-Induced Melting of (100)-Oriented Nitromethane: Energy Partitioning and Vibrational Mode Heating. *J. Chem. Phys.* **2009**, *131*, 224513.
- (2) Kabadi, V. N.; Rice, B. M. Molecular Dynamics Simulations of Normal Mode Vibrational Energy Transfer in Liquid Nitromethane. *J. Phys. Chem. A* **2004**, *108*, 532–540.
- (3) Rom, N.; Zybin, S. V.; van Duin, A. C. T.; Wang, A. G., III; Zeiri, Y.; Katz, G.; Kosloff, R. Density-Dependent Liquid Nitromethane Decomposition: Molecular Dynamics Simulations Based on ReaxFF. *J. Phys. Chem. A* **2011**, *115*, 10181–10202.
- (4) Guo, F.; Cheng, X.-L.; Zhang, H. Reactive Molecular Dynamics Simulation of Solid Nitromethane Impact on (010) Surfaces Induced and Nonimpact Thermal Decomposition. *J. Phys. Chem. A* **2012**, *116*, 3514–3520.
- (5) He, L.; Sewell, T. D.; Thompson, D. L. Molecular Dynamics Simulations of Shock Waves in Oriented Nitromethane Single Crystals. *J. Chem. Phys.* **2011**, *134*, 124506.
- (6) Gruzdkov, Y. A.; Gupta, Y. M. Emission and Fluorescence Spectroscopy To Examine Shock-Induced Decomposition in Nitromethane. *J. Phys. Chem. A* **1998**, *102*, 8325–8332.
- (7) Blais, N. C.; Engelke, R.; Sheffield, S. A. Mass Spectroscopic Study of the Chemical Reaction Zone in Detonating Liquid Nitromethane. *J. Phys. Chem. A* **1997**, *101*, 8285–8295.
- (8) Wang, J.; Brower, K. R.; Naud, D. L. Effect of Pressure on the Thermolysis of Nitroalkanes in Solution. *J. Org. Chem.* **1997**, *62*, 9048–9054.
- (9) Citroni, M.; Bini, R.; Pagliai, M.; Cardini, G.; Schettino, V. Nitromethane Decomposition under High Static Pressure. *J. Phys. Chem. B* **2010**, *114*, 9420–9428.
- (10) Kuklja, M. M.; Aduiev, B. P.; Aluker, E. D.; Krasheninina, V. I.; Krechetov, A. G.; Mitrofanov, A. Y. Role of Electronic Excitations in Explosive Decomposition of Solids. *J. Appl. Phys.* **2001**, *89*, 4156–4166.
- (11) Guo, Y. Q.; Greenfield, M.; Bhattacharya, A.; Bernstein, E. R. On the Excited Electronic State Dissociation of Nitramine Energetic Materials and Model Systems. *J. Chem. Phys.* **2007**, *127*, 154301.
- (12) Cottrell, T. L.; Graham, T. E.; Reid, T. J. The Thermal Decomposition of Nitromethane. *Trans. Faraday Soc.* **1951**, *47*, 584–590.
- (13) Bykhalo, A. I.; Zhuzhukalo, E. V.; Kovalskii, N. G.; Kolomiiskii, A. N.; Korobov, V. V.; Rozhkov, A. D.; Yudin, A. I. Initiation of PETN by High-Power Laser Radiation. *Combust., Explos. Shock Waves* **1985**, *21*, 481–483.
- (14) Tarzhanov, V. I.; Zinchenko, A. D.; Sdobnov, V. I.; Tokarev, B. B.; Pogrebov, A. I.; Volkova, A. A. Laser Initiation of PETN. *Combust., Explos. Shock Waves* **1996**, *32*, 454–459.
- (15) Aluker, E. D.; Krechetov, A. G.; Mitrofanov, A. Y.; Nurmukhametov, D. R. Photochemical and Photothermal Dissociation of PETN During Laser Initiation. *Russ. J. Phys. Chem. B* **2011**, *5*, 658–660.
- (16) Greenfield, M. T.; McGrance, S. D.; Bolme, C. A.; Bjorgaard, J. A.; Nelson, T. R.; Tretiak, S.; Scharff, R. J. Photoactive High Explosives: Linear and Nonlinear Photochemistry of Petrin Tetrazine Chloride. *J. Phys. Chem. A* **2015**, *119*, 4846–4855.
- (17) Brown, H. W.; Pimentel, G. C. Photolysis of Nitromethane and of Methyl Nitrite in an Argon Matrix; Infrared Detection of Nitroxyl, HNO. *J. Chem. Phys.* **1958**, *29*, 883–888.
- (18) Napier, I. M.; Norrish, R. G. W. The Photolysis and Pyrolysis of Nitromethane and Methyl Nitrite. *Proc. R. Soc. London, Ser. A* **1967**, *299*, 317–336.
- (19) Kwok, H. S.; He, G. Z.; Sparks, R. K.; Lee, Y. T. On the Photodissociation of Nitromethane at 266 nm. *Int. J. Chem. Kinet.* **1981**, *13*, 1125–1131.
- (20) Wodtke, A. M.; Hints, E. J.; Lee, Y. T. The Observation of CH₃O in the Collision Free Multiphoton Dissociation of CH₃NO₂. *J. Chem. Phys.* **1986**, *84*, 1044–1045.
- (21) Engelke, R.; Earl, W. L.; Rohlfling, C. M. Production of the Nitromethane Anion by UV Irradiation: Its effect on Detonation Sensitivity. *J. Phys. Chem.* **1986**, *90*, 545–547.
- (22) Rajchenbach, C.; Jonusauskas, G.; Rulliere, C. Direct Observation of the Photodecomposition of Liquid Nitromethane Under UV Photolysis by Sub-Picosecond Time-Resolved CARS Experiments. *Chem. Phys. Lett.* **1995**, *231*, 467–475.
- (23) Kilic, H. S.; Ledingham, K. W. D.; Kosmidis, C.; McCanny, T.; Singhal, R. P.; Wang, S. L.; Smith, D. J.; Langley, A. J.; Shaikh, W. Multiphoton Ionization and Dissociation of Nitromethane Using Femtosecond Laser Pulses at 375 and 750 nm. *J. Phys. Chem. A* **1997**, *101*, 817–823.
- (24) Guo, Y. Q.; Bhattacharya, A.; Bernstein, E. R. Photodissociation Dynamics of Nitromethane at 226 and 271 nm at Both Nanosecond and Femtosecond Time Scales. *J. Phys. Chem. A* **2009**, *113*, 85–96.
- (25) Goebbert, D. J.; Khuseynov, D.; Sanov, A. Photodissociation of Nitromethane Cluster Anions. *J. Chem. Phys.* **2010**, *133*, 084311.
- (26) Roszak, S.; Kaufman, J. J. Ab Initio Multiple Reference Double-Excitation Configuration-Interaction Ground and Excited State Potential Curves for Nitromethane Decomposition. *J. Chem. Phys.* **1991**, *94*, 6030.
- (27) Arenas, J. F.; Otero, J. C.; Pelaez, D.; Soto, J. The Ground and Excited State Potential Energy Surfaces of Nitromethane Related to its Dissociation Dynamics After Excitation at 193 nm. *J. Chem. Phys.* **2003**, *119*, 7814–7823.
- (28) Arenas, J. F.; Oteri, J. C.; Pelaez, D.; Soto, J. Role of Surface Crossings in the Photochemistry of Nitromethane. *J. Chem. Phys.* **2005**, *122*, 084324.
- (29) Ngyuen, M. T.; Le, H. T.; Hajgato, B.; Veszpremi, T.; Lin, M. C. Nitromethane-Methyl Nitrite Rearrangement: A Persistent Discrepancy Between Theory and Experiment. *J. Phys. Chem. A* **2003**, *107*, 4286–4291.
- (30) Dey, A.; Fernando, R.; Abeysekera, C.; Homayoon, Z.; Bowman, J. M.; Suits, A. G. Photodissociation Dynamics of Nitromethane and Methyl Nitrite by Infrared Multiphoton Dissociation Imaging with Quasiclassical Trajectory Calculations: Signatures of the Roaming Pathway. *J. Chem. Phys.* **2014**, *140*, 054305.
- (31) Mialocq, J. C.; Stephenson, J. C. Picosecond Laser-Induced Fluorescence Study of the Collisionless Photodissociation of Nitrocompounds at 266 nm. *Chem. Phys.* **1986**, *106*, 281–291.
- (32) Blais, N. C. Photofragmentation of Nitromethane in a Molecular Beam at 193 nm. *J. Chem. Phys.* **1983**, *79*, 1723–1731.
- (33) Nelson, T.; Fernandez-Alberti, S.; Chernyak, V.; Roitberg, A. E.; Tretiak, S. Nonadiabatic Excited-State Molecular Dynamics Modeling of Photoinduced Dynamics in Conjugated Molecules. *J. Phys. Chem. B* **2011**, *115*, 5402–5414.
- (34) Nelson, T.; Fernandez-Alberti, S.; Roitberg, A. E.; Tretiak, S. Nonadiabatic Excited-State Molecular Dynamics: Modeling Photochemistry in Organic Conjugated Materials. *Acc. Chem. Res.* **2014**, *47*, 1155–1164.
- (35) Greenfield, M.; McGrane, S. D.; Moore, D. S. Control of cis-Stilbene Photochemistry Using Shaped Ultraviolet Pulses. *J. Phys. Chem. A* **2009**, *113*, 2333–2339.
- (36) Nelson, T.; Fernandez-Alberti, S.; Chernyak, V.; Roitberg, A. E.; Tretiak, S. Nonadiabatic Excited-State Molecular Dynamics: Numerical Tests of Convergence and Parameters. *J. Chem. Phys.* **2012**, *136*, 054108.
- (37) Fernandez-Alberti, S.; Roitberg, A.; Nelson, T.; Tretiak, S. Identification of Unavoided Crossings in Nonadiabatic Photoexcited Dynamics Involving Multiple Electronic States in Polyatomic Conjugated Molecules. *J. Chem. Phys.* **2012**, *137*, 014512.
- (38) Nelson, T.; Fernandez-Alberti, S.; Roitberg, A. E.; Tretiak, S. Artifacts Due to Trivial Unavoided Crossings in the Modeling of

Photoinduced Energy Transfer Dynamics in Extended Conjugated Molecules. *Chem. Phys. Lett.* **2013**, *590*, 208–213.

(39) Nelson, T.; Fernandez-Alberti, S.; Roitberg, A. E.; Tretiak, S. Nonadiabatic Excited-State Molecular Dynamics: Treatment of Electronic Decoherence. *J. Chem. Phys.* **2013**, *138*, 224111.

(40) Tully, J. Molecular Dynamics with Electronic Transitions. *J. Chem. Phys.* **1990**, *93*, 1061–1071.

(41) Hammes-Schiffer, S.; Tully, J. C. Proton-Transfer in Solution - Molecular-Dynamics with Quantum Transitions. *J. Chem. Phys.* **1994**, *101*, 4657–4667.

(42) Tretiak, S.; Isborn, C.; Niklasson, A.; Challacombe, M. Representation Independent Algorithms for Molecular Response Calculations in Time-Dependent Self-Consistent Field Theories. *J. Chem. Phys.* **2009**, *130*, 054111.

(43) Tretiak, S.; Chernyak, V.; Mukamel, S. Recursive Density-Matrix-Spectral-Moment Algorithm for Molecular Nonlinear Polarizabilities. *J. Chem. Phys.* **1996**, *105*, 8914–8928.

(44) Furche, F.; Ahlrichs, R. Adiabatic Time-Dependent Density Functional Methods for Excited State Properties. *J. Chem. Phys.* **2002**, *117*, 7433–7447.

(45) Send, R.; Furche, F. First-Order Nonadiabatic Couplings from Time-Dependent Hybrid Density Functional Response Theory: Consistent Formalism, Implementation, and Performance. *J. Chem. Phys.* **2010**, *132*, 044107.

(46) Tavernelli, I.; Curchod, B. F. E.; Laktionov, A.; Rothlisberger, U. Nonadiabatic Coupling Vectors for Excited States within Time-Dependent Density Functional Theory in the Tamm-Dancoff Approximation and Beyond. *J. Chem. Phys.* **2010**, *133*, 194104.

(47) Tretiak, S.; Chernyak, V.; Mukamel, S. Two-Dimensional Real-Space Analysis of Optical Excitations in Acceptor-Substituted Carotenoids. *J. Am. Chem. Soc.* **1997**, *119*, 11408–11419.

(48) Tretiak, S.; Chernyak, V.; Mukamel, S. Collective Electronic Oscillators for Nonlinear Optical Response of Conjugated Molecules. *Chem. Phys. Lett.* **1996**, *259*, 55–61.

(49) Thouless, D. J. *The Quantum Mechanics Of Many-Body Systems*; Academic Press: New York, 1972.

(50) Dewar, M. J. S.; Zorbach, E. G.; Healy, E. F.; Stewart, J. J. P. AM1: A new general purpose quantum mechanical molecular model. *J. Am. Chem. Soc.* **1985**, *107*, 3902–3909.

(51) Manaa, M. R.; Fried, L. E. Intersystem Crossings in Model Energetic Materials. *J. Phys. Chem. A* **1999**, *103*, 9349–9354.

(52) Paterlini, M.; Ferguson, D. Constant Temperature Simulations using the Langevin Equation with Velocity Verlet Integration. *Chem. Phys.* **1998**, *236*, 243–252.

(53) Tretiak, S.; Mukamel, S. Density Matrix Analysis and Simulation of Electronic Excitations in Conjugated and Aggregated Molecules. *Chem. Rev.* **2002**, *102*, 3171–3212.

(54) Frisch, M. J.; Trucks, G. W.; Schlegel, H. B.; Scuseria, G. E.; Robb, M. A.; Cheeseman, J. R.; Scalmani, G.; Barone, V.; Mennucci, B.; Petersson, G. A.; Nakatsuji, H.; Caricato, M.; Li, X.; Hratchian, H. P.; Izmaylov, A. F.; Bloino, J.; Zheng, G.; Sonnenberg, J. L.; Hada, M.; Ehara, M.; Toyota, K.; Fukuda, R.; Hasegawa, J.; Ishida, M.; Nakajima, T.; Honda, Y.; Kitao, O.; Nakai, H.; Vreven, T.; Montgomery, J. A., Jr.; Peralta, J. E.; Ogliaro, F.; Bearpark, M.; Heyd, J. J.; Brothers, E.; Kudin, K. N.; Staroverov, V. N.; Kobayashi, R.; Normand, J.; Raghavachari, K.; Rendell, A.; Burant, J. C.; Iyengar, S. S.; Tomasi, J.; Cossi, M.; Rega, N.; Millam, J. M.; Klene, M.; Knox, J. E.; Cross, J. B.; Bakken, V.; Adamo, C.; Jaramillo, J.; Gomperts, R.; Stratmann, R. E.; Yazyev, O.; Austin, A. J.; Cammi, R.; Pomelli, C.; Ochterski, J. W.; Martin, R. L.; Morokuma, K.; Zakrzewski, V. G.; Voth, G. A.; Salvador, P.; Dannenberg, J. J.; Dapprich, S.; Daniels, A. D.; Farkas, O.; Foresman, J. B.; Ortiz, J. V.; Cioslowski, J.; Fox, D. J. *Gaussian 09*, revision D.01; Gaussian, Inc.: Wallingford, CT, 2009.

(55) Bayliss, N. S.; McRae, E. G. Solvent Effects in the Spectra of Acetone, Crotonaldehyde, Nitromethane and Nitrobenzene. *J. Phys. Chem.* **1954**, *58*, 1006–1011.

(56) Nagakura, S. Ultra-violet Absorption Spectra and π -Electron Structures of Nitromethane and the Nitromethyl Anion. *Mol. Phys.* **1960**, *3*, 152–162.

(57) Greenfield, M. T.; McGrane, S. D.; Brown, K. E.; Moore, D. S.; Scharff, R. J. Towards Optical Control of Energetic Materials. Fifteenth International Detonation Symposium; Office of Naval Research, San Francisco, CA, July 13–18, **2014**, pp 273–283.

(58) Constantinou, C. P.; Pereira, C.; Chaudhri, M. M. Increased Concentration of the Nitromethyl Anion in Nitromethane-Amine Mixtures. *Propellants, Explos., Pyrotech.* **1995**, *20*, 200–205.

(59) Triggs, N. E.; Zahedi, M.; Nibler, J. W.; DeBarber, P.; Valentini, J. J. High Resolution Study of the N1 Vibration of Ch3 by Coherent Raman Photofragment Spectroscopy. *J. Chem. Phys.* **1992**, *96*, 1822–1831.

(60) Jacox, M. E. Matrix Isolation Study of the Infrared Spectrum and Structure of the Ch 3 Free Radical. *J. Mol. Spectrosc.* **1977**, *66*, 272–287.

(61) Kelly, P.; Westre, S. G. Resonance Raman Spectroscopy of the Methyl Radical. *Chem. Phys. Lett.* **1988**, *151*, 253–257.

(62) Crofton, M. W.; Kreiner, W. A.; Jagod, M. F.; Rehfuss, B. D.; Oka, T. Observation of the Infrared Spectrum of Methyl Cation CH_3^+ . *J. Chem. Phys.* **1985**, *83*, 3702–3703.

(63) Snelson, A. Infrared Matrix Isolation Spectrum of the Methyl Radical Produced by Pyrolysis of Methyl Iodide and Dimethyl Mercury. *J. Phys. Chem.* **1970**, *74*, 537–544.

(64) Andrews, L.; Pimentel, G. C. Infrared Spectrum of the Methyl Radical in Solid Argon. *J. Chem. Phys.* **1967**, *47*, 3637–3644.

(65) Crofton, M. W.; Jagod, M. F.; Rehfuss, B. D.; Kreiner, W. A.; Oka, T. Infrared spectroscopy of carbo-ions. III. ν_3 band of methyl cation CH_3^+ . *J. Chem. Phys.* **1988**, *88*, 666–678.

(66) Rook, F. L.; Jacox, M. E. The Vibrational Spectra of Methyl and Methyl-D 3 Nitrite. *J. Mol. Spectrosc.* **1982**, *93*, 101–116.

(67) Tarte, P. Rotational Isomerism as a General Property of Alkyl Nitrites. *J. Chem. Phys.* **1952**, *20*, 1570–1575.

(68) Rook, F. L. Preparation, Vapor Pressure, and Infrared Spectrum of Methyl Nitrite. *J. Chem. Eng. Data* **1982**, *27*, 72–73.

(69) Vorsa, V.; Campagnola, P. J.; Nandi, S.; Larsson, M.; Lineberger, W. C. Photofragmentation of $\text{I}_2 \cdot \text{Ar}_n$ Clusters: Observation of Metastable Isomeric Ionic Fragments. *J. Chem. Phys.* **1996**, *105*, 2298–2308.

(70) Zadoyan, R.; Li, Z.; Martens, C. C.; Apkarian, V. A. The Breaking and Remaking of a Bond: Caging of I_2 in Solid Kr. *J. Chem. Phys.* **1994**, *101*, 6648–6657.